**Structural Engineering and Mechanics**, *Vol. 62, No. 6 (2017) 725-737*
DOI: https://doi.org/10.12989/sem.2017.62.6.725


# Short- and long-term analyses of shear lag in RC box girders considering axial equilibrium

Yiqiang Xiang* and Xiaoyang He[a]

*Department of Civil Engineering, Zhejiang University, Hangzhou 310058, China*

*(Received September 29, 2016, Revised May 11, 2017, Accepted May 23, 2017)*

**Abstract.** An analytical method considering axial equilibrium is proposed for the short- and long-term analyses of shear lag effect in reinforced concrete (RC) box girders. The axial equilibrium of box girders is taken into account by using an additional generalized displacement, referred to as the longitudinal displacement of the web. Three independent shear lag functions are introduced to describe different shear lag intensities of the top, bottom, and cantilever plates. The time-dependent material properties of the concrete are simulated by the age-adjusted effective modulus method (AEMM), while the reinforcement is assumed to behave in a linear-elastic fashion. The differential equations are derived based on the longitudinal displacement of the web, the vertical displacement of the cross section, and the shear lag functions of the flanges. The time-dependent expressions of the generalized displacements are then deduced for box girders subjected to uniformly distributed loads. The accuracy of the proposed method is validated against the finite element results regarding the short- and long-term responses of a simply-supported RC box girder. Furthermore, creep analyses considering and neglecting shrinkage are performed to quantify the time effects on the long-term behavior of a continuous RC box girder. The results show that the proposed method can well evaluate both the short- and long-term behavior of box girders, and that concrete shrinkage has a considerable impact on the concrete stresses and internal forces, while concrete creep can remarkably affect the long-term deflections.

**Keywords:** RC box girder; shear lag; creep; shrinkage; axial equilibrium; generalized displacement

## 1. Introduction

Concrete box girders have been widely used in modern bridges due to their large bending and torsional stiffness. However, excessive mid-span deflections and cracking, which can seriously affect the structural safety and serviceability, have been commonly observed in numerous concrete box girder bridges around the world (Takacs 2002, Yang 2007a, Wen 2011, Sousa *et al*. 2012). The unexpected phenomena and even structural collapse may result from many factors, for instance, concrete creep and shrinkage, shear lag effect, prestressing relaxation, defects in the design and construction processes (Bazant *et al*. 2012a, Zhang and Lin 2014a, Lou *et al*. 2016, Xiang *et al*. 2011). Accordingly, it is necessary to accurately predict the responses of box girder bridges in the life cycle.

The time-dependent behavior of concrete structures has been generally analyzed by many scholars according to the traditional beam theory, which cannot realistically describe the shear lag of box sections (Robertson 2005, Yang 2007b, Pan *et al*. 2011, Granata *et al*. 2013, Elbadry *et al*. 2014, Sousa *et al*. 2014, Lou *et al*. 2015a, b). For the purpose of improving the prediction accuracy, some researchers have further established three-dimensional finite element models consisting of shell or solid elements to capture shear lag effect. Kristek and Bazant (1987) observed that the shear lag can significantly affect the long-term deflections and stresses. Compared with the results obtained by the solid element model, the analysis using the beam element model may underestimate the long-term deflection by about 20% (Bazant *et al*. 2012b). Norachan *et al.* (2014) achieved the long-time behavior of a segmentally constructed box girder bridge utilizing hexahedral elements. In accordance with the monitoring data and the probabilistic shell element models, the deflection control strategies were made for box girder bridges (Guo and Chen 2016). Besides, Malm and Sundquist (2010) interpreted the influence of the non-uniform creep and shrinkage on the time-varying deflections and stresses. And Xiang and He (2015) concluded that the non-uniform creep and shrinkage may lead to cracking in the bottom flange. Although the shell or solid element method can effectively simulate the shear lag, it is time-consuming and may be beyond the reach of an average engineer. As seen in literature, few studies proposed the simplified methods for the time-dependent analysis of shear lag in concrete box girders. Thus it seems essential to seek a simplified and analytical method, taking into account shear lag effect, and creep and shrinkage of concrete.

Extensive studies on the analytical approaches to determine the shear lag have been conducted for decades. After Reissner (1946) first adopted a variation method based on the principle of minimum potential energy to analyze the shear lag in a rectangular box beam, the method

*Corresponding author, Professor
E-mail: xiangyiq@zju.edu.cn
[a]Ph.D. Student
E-mail: hxysunrise@zju.edu.cn



ISSN: 1225-4568 (Print), 1598-6217 (Online)

was extended to the shear lag analysis of box girders with cantilever plates (Dezi and Mentrasti 1985, Wu *et al*. 2003, Zhou 2010). However, those studies are generally based on the assumption that the neutral axis of box girders coincides with the centroidal axis. The assumption may not satisfy the axial equilibrium condition which is critical for accuracy of the shear lag analysis. To realize the axial balance of box girders, Zhang (2012), and Lin and Zhao (2011a, b) added correction terms to the shear lag displacement function and the longitudinal displacement, respectively. Nevertheless, the physical meanings of additional correction terms are not clear, and may be limited to practical applications.

This paper presents a simplified model considering axial equilibrium for the short- and long-term analyses of shear lag in RC box girders. The longitudinal displacement of the web is added to the displacement field to satisfy the axial equilibrium condition. To consider the different shear lag intensities of the flanges in box girders, three independent shear lag functions are chosen for the top, bottom and cantilever plates, respectively. The differential equations and boundary conditions can be established by applying the virtual work theorem and partial integration. The closed-form solutions of the differential equations are then derived for box girders subjected to uniformly distributed loads. The finite element analysis of a simply-supported RC box girder is performed to verify the effectiveness and reliability of the proposed method. Finally, a comparative study of the results obtained by the creep analyses with and without shrinkage is carried out for a better understanding of the effects of creep and shrinkage on the time-dependent behavior of a continuous RC box girder.

## 2. Analytical model

A thin-walled RC box girder with trapezoidal cross section is shown in Fig. 1. A coordinate system {*O*; *X*, *Y*, *Z*} is introduced, with the *Z* axis parallel to the axis of the undeformed box girder. Based on the assumption of a symmetric cross section, the coordinate plane *YZ* is also selected to coincide with the symmetry plane of the girder.

### *2.1 Displacement and strain fields*

For the sake of establishing an analytical model accounting for the shear lag effect in concrete box girders, the following assumptions are given:

(1) The external loads are located so as to avoid torsion, distortion and transverse bending of the cross section;

(2) Plane-section hypothesis is applied to the webs, so the shear deformation is not considered for the webs;

(3) The shear lag effect due to the in-plane shear deformation is taken into account in the flanges;

(4) No bond slip can occur between the reinforcing bars and the surrounding concrete.

To satisfy the axial equilibrium condition of the box girder, the longitudinal displacement of the web is added to the displacement field, which is different from the methods in the previous literature. For describing the different shear lag intensities of the slabs, three independent shear lag functions can be chosen for the top, bottom and cantilever slabs, respectively (Luo *et al*. 2004). The deformation process of the girder from time $t_0$ to $t$ ($t > t_0$) is depicted in Fig. 2. Therefore, the displacement field can be obtained as follows

$$\mathbf{u}_i(x,y,z;t) = v(z;t)\mathbf{j} + [w(z;t) - yv'(z;t) + f_i(z;t)\psi_i(x)]\mathbf{k}; i = 1,2,3 \tag{1a}$$

$$\mathbf{u}_4(x,y,z;t) = v(z;t)\mathbf{j} + [w(z;t) - yv'(z;t)]\mathbf{k} \tag{1b}$$

where **j**, **k** are the unit vectors along the axes *Y* and *Z*, respectively; the prime denotes a derivative with respect to the variable *z*; the subscript *i*=1, 2, 3 represents the top, bottom and cantilever slabs, respectively; *v* is the deflection of the box girder; *w* is the longitudinal displacement of the web; $f_i$ and $\psi_i$ are the shear lag functions and the shear lag displacement functions of the top, bottom and cantilever slabs, respectively.

According to the displacement field defined in Eq. (1), the strain field can be calculated, and the following non zero components are expressed as

$$\varepsilon_i = w' - yv'' + f_i'\psi_i; i = 1,2,3 \tag{2a}$$

$$\gamma_i = f_i\psi_{i,x}; i = 1,2,3 \tag{2b}$$

$$\varepsilon_4 = w' - yv'' \tag{2c}$$

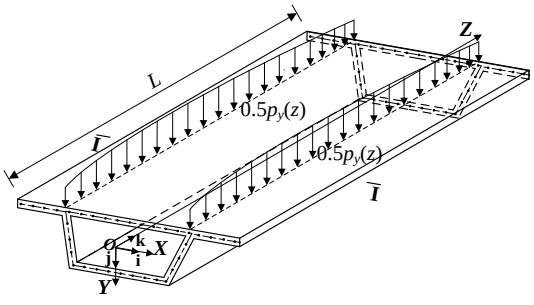


(a) Coordinate system and load

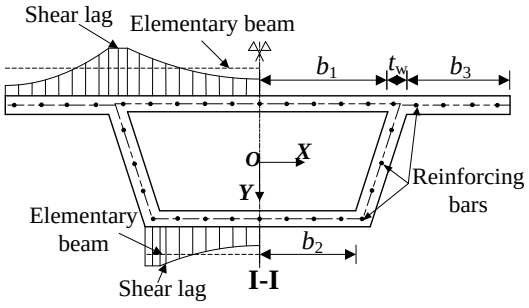


(b) Cross section

Fig. 1 Thin-walled RC box girder

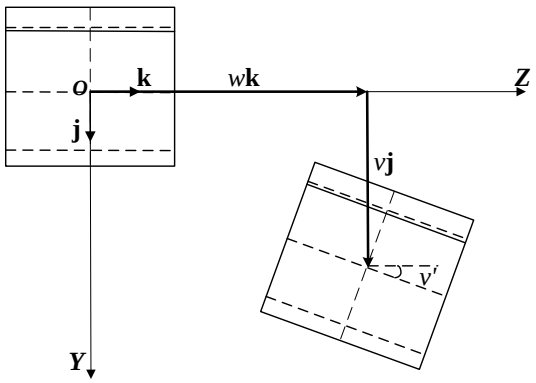


Fig. 2 Cross-section displacement components

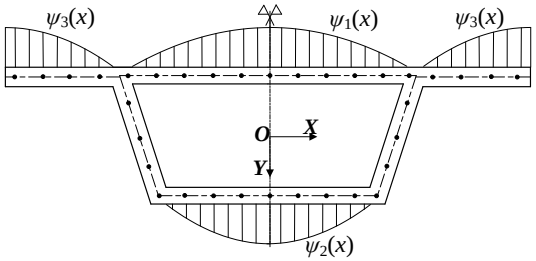


Fig. 3 Shear lag displacement functions

where $\varepsilon_i$ ($i$=1, 2, 3, 4) represent the axial strains in the top, bottom and cantilever plates, and the webs, respectively; $\gamma_i$ define the shear strains in the top, bottom and cantilever plates, respectively; the comma represents partial derivative with respect to variable $x$.

The shear lag displacement functions, which may significantly affect the accuracy of the shear lag analysis, must be carefully selected. As shown in Fig. 3, the functions should be chosen in the light of the following principles: (1) for the thin-walled structures, they can be only related to the variable $x$ (Dezi *et al*. 2001); (2) they are symmetric with respect to the $Y$ axis and continuous along the slab width; (3) at the edge of the cantilever slabs and at the center of the top and bottom slabs, $\psi_{i,x}$=0 can guarantee zero shear stresses; (4) at the intersections of the webs and the flanges, $\psi_i$=0 can be required by the plane-section hypothesis for the webs. The quadratic parabola was proved to be the reasonable curve of the shear lag displacement function (Zhang and Lin 2014b). Thus, $\psi_i$ in this paper can be chosen as

$$\psi_1(x) = -(1 - x^2 / b_1^2) \tag{3a}$$

$$\psi_2(x) = 1 - x^2 / b_2^2 \tag{3b}$$

$$\psi_3(x) = -[1 - (b_1 + b_3 + t_w - x)^2 / b_3^2] \tag{3c}$$

where $2b_1$, $2b_2$ and $b_3$ denote the width of the top, bottom and cantilever plates, respectively; $t_w$ is the web width.

### 2.2 Constitutive laws of materials

#### 2.2.1 Concrete

According to the assumption of linear creep, CEB-FIP model code 1990 (1993) presented the integral-type constitutive law of concrete under variable stresses as

$$\varepsilon_c(t) = \sigma_c(t_0) J(t, t_0) + \int_{t_0}^{t} J(t, \theta) \mathrm{d}\sigma_c(\theta) + \varepsilon_{sh}(t) \tag{4a}$$

$$\gamma_c(t) = 2(1+\mu)[\tau(t_0) J(t, t_0) + \int_{t_0}^{t} J(t, \theta) \mathrm{d}\tau_c(\theta)] \tag{4b}$$

where $t$ is the age of the concrete at the moment considered; $t_0$ is the age of the concrete at intial loading; $\varepsilon_c$ and $\gamma_c$ are the axial and shear strains in the concrete, respectively; $\varepsilon_{sh}(t)$ is the shrinkage strain at time $t$; $\sigma_c$ and $\tau_c$ are the axial and shear stresses in the concrete, respectively; $J(t,\theta)$ is defined as the strain at time $t$ caused by a constant unit stress acting from time $\theta$ to time $t$; $\mu$ is the Poisson ratio of the concrete considered to be constant in time (Gara *et al*. 2009).

Analytical solutions for the long-term behavior of concrete structures cannot be obtained by adopting the constitutive laws defined in Eq. (4). In addition, the results obtained by AEMM are more accurate than those by other simplified methods for creep analysis, for example, the effective modulus method and the mean stress method. For gaining the closed-form solutions, AAEM (Bazant 1972) is utilized to simplify Eq. (4) in this paper. The stress history is considered by introducing the aging coefficient in this method, which only involves the concrete stresses at times $t$ and $t_0$. Moreover, it is assumed that the creep behavior of the concrete is identical in compression and tension (Gara *et al*. 2010, Gilbert and Ranzi 2011). The concrete is supposed to be uncracked even in the tension regions (Dezi *et al*. 2003). This assumption can be made only for the beneficial effect of prestressing. However, the problem linearity permits the uncoupling of effects under different actions. Therefore, the calculated results can show time effects on the shear lag in reinforced or prestressed concrete box girders subjected to external loads.

The time-dependent stress-strain relationships are considered for the concrete

$$\sigma_{ic0} = E_{c0}\varepsilon_{ic0}, \sigma_{ict} = E_{ct}(\varepsilon_{ict} - \varepsilon_{sh}) + \phi\sigma_{ic0}; i = 1, 2, 3, 4 \tag{5a}$$

$$\tau_{ic0} = G_{c0}\gamma_{ic0}, \tau_{ict} = G_{ct}\gamma_{ict} + \phi\tau_{ic0}; i = 1, 2, 3 \tag{5b}$$

where

$$G_{c\varsigma} = \frac{E_{c\varsigma}}{2(1+\mu)}, E_{ct} = \frac{E_{c0}}{1+\chi\varphi}, \phi = \frac{(\chi-1)\varphi}{1+\chi\varphi} \tag{6}$$

and $\zeta$=0, $t$ represents times $t_0$ and $t$, respectively; $\sigma_{ic\zeta}$ and $\tau_{ic\zeta}$ are the axial and shear stresses in the concrete, respectively; $\varepsilon_{ic\zeta}$ and $\gamma_{ic\zeta}$ are the axial and shear strains in the concrete, respectively; $E_{c0}$ and $G_{c0}$ are the Young's and shear moduli of the concrete at time $t_0$, respectively; $E_{ct}$ and $G_{ct}$ are the age-adjusted effective moduli of the concrete at time $t$; $\varphi$ is the creep coefficient at time $t$; $\chi$ is the aging coefficient at

time *t*.

### 2.2.2 Reinforcing steel

The reinforcements can be assumed to behave in a linear elastic manner. The following one-dimensional constitutive law is adopted

$$\sigma_{ir\zeta} = E_r \varepsilon_{ir\zeta}; i = 1, 2, 3, 4 \tag{7}$$

where $\sigma_{ir\zeta}$ and $\varepsilon_{ir\zeta}$ are the axial stress and the axial strain in the reinforcements, respectively; $E_r$ is the Young's modulus of the reinforcements.

### 2.3 Global balance condition

The longitudinal displacement of the web *w*, the vertical deflection *v*, and the shear lag functions $f_i$ are defined as unknown variables. By assuming that the box girder is subjected to the body and surface forces, **b** and **s**, based on the principle of virtual work, the global balance condition at time *t* can be obtained as

$$\begin{aligned}&\sum_{i=1}^{4}\int_L\int_{A_i}\sigma_i\delta\varepsilon_i \mathrm{d}A\mathrm{d}z + \sum_{i=1}^{3}\int_L\int_{A_i}\tau_i\delta\gamma_i \mathrm{d}A\mathrm{d}z = \\ &\sum_{i=1}^{4}\int_L\int_{A_i}\mathbf{b}\cdot\delta\mathbf{u}\mathrm{d}A\mathrm{d}z + \sum_{i=1}^{4}\int_L\int_{\Gamma A_i}\mathbf{s}\cdot\delta\mathbf{u}\mathrm{d}x\mathrm{d}z + \sum_{i=1}^{4}\int_{A_i}\mathbf{s}\cdot\delta\mathbf{u}\mathrm{d}A\Big|_0^L\end{aligned} \tag{8}$$

in which $A_i$ and $\Gamma A_i$ represent the cross-sections and contours of the webs, the top, bottom and cantilever slabs, respectively; *L* is the span of the box girder.

By virtue of Eq. (1) for the displacement field, (2) for the strain field, and (5) and (7) for the constitutive laws, Eq. (8) can be re-written in the following form

$$\begin{aligned}&\int_L (N\delta w' - M\delta v'' + \sum_{i=1}^{3} W_i\delta f_i' + \sum_{i=1}^{3} Q_{ic}\delta f_i)\mathrm{d}z = \\ &\int_L (p_z\delta w + p_y\delta v - q\delta v' + \sum_{i=1}^{3} g_i\delta f_i)\mathrm{d}z + \\ &(N^*\delta w + V^*\delta v - M^*\delta v' + \sum_{i=1}^{3} W_i^*\delta f_i)\Big|_0^L\end{aligned} \tag{9}$$

where

$$N = w'EA_t - v''EB_t + \sum_{i=1}^{3} f_i'EA_{i\psi t} - \varepsilon_{sh}EA_{ct} + \phi N_{c0} \tag{10a}$$

$$M = w'EB_t - v''EI_t + \sum_{i=1}^{3} f_i'EB_{i\psi t} - \varepsilon_{sh}EB_{ct} + \phi M_{c0} \tag{10b}$$

$$W_i = w'EA_{i\psi t} - v''EB_{i\psi t} + f_i'EI_{i\psi t} - \varepsilon_{sh}EA_{ic\psi t} + \phi W_{ic0}; \quad i = 1, 2, 3 \tag{10c}$$

$$Q_{ic} = f_i GI_{id\psi t} + \phi Q_{ic0}; i = 1, 2, 3 \tag{10d}$$

are the cross-section stress resultants at time *t* (*N* and *M* are the axial force and the moment resisted by the whole cross section at time *t*, respectively; $W_i$ represent the bi-moments resisted by the top, bottom and cantilever slabs at time *t*, respectively; $Q_{ic}$ are the bi-shears resisted by the concrete in the top, bottom and cantilever slabs at time *t*, respectively); while

$$p_z = \sum_{i=1}^{4}\left(\int_{\Gamma A_{ic}} s_{zi}\mathrm{d}x + \int_{A_{ic}} b_{zi}\mathrm{d}A + \int_{\Gamma A_{ir}} s_{zi}\mathrm{d}x + \int_{A_{ir}} b_{zi}\mathrm{d}A\right) \tag{11a}$$

$$p_y = \sum_{i=1}^{4}\left(\int_{\Gamma A_{ic}} s_{yi}\mathrm{d}x + \int_{A_{ic}} b_{yi}\mathrm{d}A + \int_{\Gamma A_{ir}} s_{yi}\mathrm{d}x + \int_{A_{ir}} b_{yi}\mathrm{d}A\right) \tag{11b}$$

$$q = \sum_{i=1}^{4}\left(\int_{\Gamma A_{ic}} s_{zi}y\mathrm{d}x + \int_{A_{ic}} b_{zi}y\mathrm{d}A + \int_{\Gamma A_{ir}} s_{zi}y\mathrm{d}x + \int_{A_{ir}} b_{zi}y\mathrm{d}A\right) \tag{11c}$$

$$g_i = \int_{\Gamma A_{ic}} s_{zi}\psi_i\mathrm{d}x + \int_{A_{ic}} b_{zi}\psi_i\mathrm{d}A + \int_{\Gamma A_{ir}} s_{zi}\psi_i\mathrm{d}x + \int_{A_{ir}} b_{zi}\psi_i\mathrm{d}A; \quad i = 1, 2, 3 \tag{11d}$$

represent the resultants of the body and surface forces applied along the girder; and

$$N^* = \sum_{i=1}^{4}\left(\int_{A_{ic}} s_{zi}\mathrm{d}A + \int_{A_{ir}} s_{zi}\mathrm{d}A\right) \tag{12a}$$

$$V^* = \sum_{i=1}^{4}\left(\int_{A_{ic}} s_{yi}\mathrm{d}A + \int_{A_{ir}} s_{yi}\mathrm{d}A\right) \tag{12b}$$

$$M^* = \sum_{i=1}^{4}\left(\int_{A_{ic}} s_{zi}y\mathrm{d}A + \int_{A_{ir}} s_{zi}y\mathrm{d}A\right) \tag{12c}$$

$$W_i^* = \int_{A_{ic}} s_{zi}\psi_i\mathrm{d}A + \int_{A_{ir}} s_{zi}\psi_i\mathrm{d}A; i = 1, 2, 3 \tag{12d}$$

denote the resultants of the surface forces applied at the girder ends.

In Eq. (10), the defined cross-sectional rigidities (with the subscript $\zeta$=0, *t* when computed at times $t_0$ and *t*, respectively) are expressed as

$$EA_{c\zeta} = \sum_{i=1}^{4}\int_{A_{ic}} E_{c\zeta}\mathrm{d}A,\ EA_{\zeta} = EA_{c\zeta} + \sum_{i=1}^{4}\int_{A_{ir}} E_r\mathrm{d}A \tag{13a}$$

$$EB_{c\zeta} = \sum_{i=1}^{4} \int_{A_{ic}} E_{c\zeta} y \mathrm{d}A,\ EB_{\zeta} = EB_{c\zeta} + \sum_{i=1}^{4} \int_{A_{ir}} E_{r} y \mathrm{d}A \tag{13b}$$

$$EI_{\zeta} = \sum_{i=1}^{4} \left( \int_{A_{ic}} E_{c\zeta} y^2 \mathrm{d}A + \int_{A_{ir}} E_{r} y^2 \mathrm{d}A \right) \tag{13c}$$

$$EA_{ic\psi\zeta} = \int_{A_{ic}} E_{c\zeta} \psi_i \mathrm{d}A; i = 1, 2, 3 \tag{13d}$$

$$EA_{i\psi\zeta} = EA_{ic\psi\zeta} + \int_{A_{ir}} E_{r} \psi_i \mathrm{d}A; i = 1, 2, 3 \tag{13e}$$

$$EB_{i\psi\zeta} = \int_{A_{ic}} E_{c\zeta} y \psi_i \mathrm{d}A + \int_{A_{ir}} E_{r} y \psi_i \mathrm{d}A; i = 1, 2, 3 \tag{13f}$$

$$EI_{i\psi\zeta} = \int_{A_{ic}} E_{c\zeta} \psi_i^2 \mathrm{d}A + \int_{A_{ir}} E_{r} \psi_i^2 \mathrm{d}A; i = 1, 2, 3 \tag{13g}$$

$$GI_{id\psi\zeta} = \int_{A_{ic}} G_{c\zeta} \psi_{i,x}^2 \mathrm{d}A; i = 1, 2, 3 \tag{13h}$$

and

$$N_{c0} = \sum_{i=1}^{4} \int_{A_{ic}} \sigma_{ic0} \mathrm{d}A \tag{14a}$$

$$M_{c0} = \sum_{i=1}^{4} \int_{A_{ic}} \sigma_{ic0} y \mathrm{d}A \tag{14b}$$

$$W_{ic0} = \int_{A_{ic}} \sigma_{ic0} \psi_i \mathrm{d}A; i = 1, 2, 3 \tag{14c}$$

$$W_{ic0} = \int_{A_{ic}} \sigma_{ic0} \psi_i \mathrm{d}A; i = 1, 2, 3 \tag{14d}$$

are the cross-section stress resultants at time $t_0$ ($N_{c0}$ and $M_{c0}$ are the axial force and the moment resisted by the concrete in the whole cross section at time $t_0$, respectively; $W_{ic0}$ and $Q_{ic0}$ denote the bi-moments and bi-shears resisted by the concrete in the flanges at time $t_0$, respectively). In Eqs. (11)-(12), $s_{zi}$ and $b_{zi}$ are the components of the surface and body forces in the $Z$ direction, respectively, while $s_{yi}$ and $b_{yi}$ are the components of the surface and body forces in the $Y$ direction, respectively.

The influence of the shear lag on the short- and long-term behavior of concrete box girders can be reflected by the bi-shears and bi-moments defined in Eqs. (10c), (10d), (14c) and (14d). Eq. (10) can also indicate that the long-term behavior of concrete structures at time $t$ is related to the short-term behavior at time $t_0$. Hence, for the purpose of conducting the long-term analysis, the short-term problem must be solved in advance. It is worth noting that the cross-section rigidities depending on the material properties of the concrete at times $t_0$ and $t$ need to be calculated for the short- and long-time analyses, respectively.

### *2.4 Governing differential equations and boundary conditions*

The governing system of differential equations and corresponding boundary conditions, describing the time-dependent behavior of shear lag effect in concrete box bridges, can be derived by integrating Eq. (9) by parts. The differential equations can be expressed as

$$N' + p_z = 0 \tag{15a}$$

$$M'' + q' + p_y = 0 \tag{15b}$$

$$W_i' - Q_{ic} + g_i = 0; i = 1, 2, 3 \tag{15c}$$

and the corresponding boundary conditions at the girder ends can be written as

$$(N - N^*)\delta w\big|_0^L = 0 \tag{16a}$$

$$(M' + q - V^*)\delta v\big|_0^L = 0 \tag{16b}$$

$$(M - M^*)\delta v'\big|_0^L = 0 \tag{16c}$$

$$(W_i - W_i^*)\delta f_i\big|_0^L = 0; i = 1, 2, 3 \tag{16d}$$

Eq. (15a) depicts the longitudinal equilibrium of the box girder; Eq. (15b) represents the vertical equilibrium of the box girder; while Eq. (15c) imposes the balance conditions between the axial stresses and the shear stresses in the flanges. Eq. (16) simultaneously contains the static and displacement boundary conditions. It is worth highlighting that only the uniform shrinkage is considered in this paper. Therefore, for concrete box girders with constant cross section, the terms related to the shrinkage strain cannot appear in Eq. (15), but only in Eq. (16).

### *2.5 Closed-form solutions*

The short- and long-term solutions considering shear lag effect are deduced for a RC box girder subjected to a uniformly vertical distributed load $p_y$. The generalized displacements at times $t_0$ and $t$ are distinguished by the subscript $\zeta$=0, $t$.

#### 2.5.1 Shear lag analysis at time $t_0$

According to the differential equations defined in Eqs. (15a) and (15b), the generalized displacements $w_0$ and $v_0$ can be expressed in terms of $f_{i0}$ as

$$w_0'' = \sum_{i=1}^{3} \omega_{i0} f_{i0}'' + \omega_{p0}(p_y z + C_0) \tag{17a}$$

$$v_0''' = \sum_{i=1}^{3} \rho_{i0} f_{i0}'' + \rho_{p0}(p_y z + C_0) \tag{17b}$$

where

$$\omega_{i0} = \frac{EB_{i\psi 0} EB_0 - EA_{i\psi 0} EI_0}{EA_0 EI_0 - EB_0^2}; i = 1, 2, 3 \tag{18a}$$

$$\rho_{i0} = \frac{EB_{i\psi 0} EA_0 - EA_{i\psi 0} EB_0}{EA_0 EI_0 - EB_0^2}; i = 1, 2, 3 \tag{18b}$$

$$\omega_{p0} = \frac{EB_0}{EA_0 EI_0 - EB_0^2} \tag{18c}$$

$$\rho_{p0} = \frac{EA_0}{EA_0 EI_0 - EB_0^2} \tag{18d}$$

and $C_0$ is an integral constant at time $t_0$.

By substituting Eq. (17) into Eq. (15c), the following group of the differential equations can be obtained and re-written in a matrix form as

$$\mathbf{L}_0 \mathbf{f}_0'' - \mathbf{M}_0 \mathbf{f}_0 = \mathbf{N}_{p0}(p_y z + C_0) \tag{19}$$

where

$$\mathbf{f}_0 = [f_{10} \quad f_{20} \quad f_{30}]^{\mathrm{T}} \tag{20a}$$

$$\mathbf{L}_0 = \begin{bmatrix} l_{110} & l_{120} & l_{130} \\ l_{210} & l_{220} & l_{230} \\ l_{310} & l_{320} & l_{330} \end{bmatrix} \tag{20b}$$

$$\mathbf{M}_0 = \mathrm{diag}(m_{10} \quad m_{20} \quad m_{30}) \tag{20c}$$

$$\mathbf{N}_{p0} = [n_{p10} \quad n_{p20} \quad n_{p30}]^{\mathrm{T}} \tag{20d}$$

The elements in Eqs. (20b), (20c) and (20d) are defined as

$$l_{ii0} = EA_{i\psi 0}\omega_{i0} - EB_{i\psi 0}\rho_{i0} + EI_{i\psi 0}; i = 1, 2, 3 \tag{21a}$$

$$l_{ji0} = EA_{j\psi 0}\omega_{i0} - EB_{j\psi 0}\rho_{i0}; i = 1, 2, 3, j = 1, 2, 3, i \neq j \tag{21b}$$

$$m_{j0} = GI_{jd\psi 0}; j = 1, 2, 3 \tag{21c}$$

$$n_{pj0} = EB_{j\psi 0}\rho_{p0} - EA_{j\psi 0}\omega_{p0}; j = 1, 2, 3 \tag{21d}$$

Based on Eq. (19), the solutions of $f_{i0}$ can be obtained as

$$f_{i0} = \sum_{\alpha=1}^{3} \xi_{i\alpha 0}(C_{(2\alpha-1)0} \operatorname{ch} \lambda_{\alpha 0} z + C_{(2\alpha)0} \operatorname{sh} \lambda_{\alpha 0} z) - \frac{n_{pi0}}{m_{i0}}(p_y z + C_0); i = 1, 2, 3 \tag{22}$$

and

$$\boldsymbol{\xi}_0 = \begin{bmatrix} \xi_{110} & \xi_{120} & \xi_{130} \\ \xi_{210} & \xi_{220} & \xi_{230} \\ \xi_{310} & \xi_{320} & \xi_{330} \end{bmatrix} \tag{23}$$

where $C_{k0}$ ($k$=1, ... , 6) are the integral constants, which can be determined by use of the boundary conditions at time $t_0$; $\lambda_{\alpha 0}^2$ ($\alpha$=1, 2, 3) are the eigenvalues of $\mathbf{L}_0^{-1}\mathbf{M}_0$; $\boldsymbol{\xi}_0$ is the matrix of the right eigenvetors of $\mathbf{L}_0^{-1}\mathbf{M}_0$.

#### 2.5.2 Shear lag analysis at time $t$

Determining the short-term response can make it possible to perform the long-term analysis. The generalized displacements $w_t$ and $v_t$ can be written in terms of $f_{it}$ as

$$w_t'' = \sum_{i=1}^{3} \omega_{it} f_{it}'' + \omega_{Nt} N_{c0}' + \omega_{Mt} M_{c0}' + \omega_{pt}(p_y z + C_t) \tag{24a}$$

$$v_t''' = \sum_{i=1}^{3} \rho_{it} f_{it}'' + \rho_{Nt} N_{c0}' + \rho_{Mt} M_{c0}' + \rho_{pt}(p_y z + C_t) \tag{24b}$$

where

$$\omega_{it} = \frac{EB_{i\psi t} EB_t - EA_{i\psi t} EI_t}{EA_t EI_t - EB_t^2}; i = 1, 2, 3 \tag{25a}$$

$$\rho_{it} = \frac{EB_{i\psi t} EA_t - EA_{i\psi t} EB_t}{EA_t EI_t - EB_t^2}; i = 1, 2, 3 \tag{25b}$$

$$\omega_{Nt} = -\frac{\phi EI_t}{EA_t EI_t - EB_t^2}, \rho_{Nt} = \frac{\phi EB_t}{EA_t EI_t - EB_t^2} \tag{25c}$$

$$\omega_{Mt} = \frac{\phi EB_t}{EA_t EI_t - EB_t^2}, \rho_{Mt} = \frac{\phi EA_t}{EA_t EI_t - EB_t^2} \tag{25d}$$

$$\omega_{pt}=\frac{EB_t}{EA_tEI_t-EB_t^2},\ \rho_{pt}=\frac{EA_t}{EA_tEI_t-EB_t^2} \tag{25e}$$

and $C_t$ is an integral constant at time $t$.

Substituting Eq. (24) into Eq. (15c) can yield the group of the differential equations, which can be expressed as

$$\mathbf{L}_t\mathbf{f}_t''-\mathbf{M}_t\mathbf{f}_t=\mathbf{N}_N N_{c0}'+\mathbf{N}_M M_{c0}'-\phi\mathbf{W}_{c0}'+\phi\mathbf{Q}_{c0}+\mathbf{N}_{pt}(p_y z+C_t) \tag{26}$$

where

$$\mathbf{f}_t=[\,f_{1t}\quad f_{2t}\quad f_{3t}\,]^{\mathrm{T}} \tag{27a}$$

$$\mathbf{L}_t=\begin{bmatrix} l_{11t} & l_{12t} & l_{13t}\\ l_{21t} & l_{22t} & l_{23t}\\ l_{31t} & l_{32t} & l_{33t}\end{bmatrix} \tag{27b}$$

$$\mathbf{M}_t=\mathrm{diag}(\,m_{1t}\quad m_{2t}\quad m_{3t}) \tag{27c}$$

$$\mathbf{N}_{pt}=[\,n_{p1t}\quad n_{p2t}\quad n_{p3t}\,]^{\mathrm{T}} \tag{27d}$$

$$\mathbf{N}_N=[\,n_{N1}\quad n_{N2}\quad n_{N3}\,]^{\mathrm{T}} \tag{27e}$$

$$\mathbf{N}_M=[\,n_{M1}\quad n_{M2}\quad n_{M3}\,]^{\mathrm{T}} \tag{27f}$$

$$\mathbf{W}_{c0}=[\,W_{1c0}\quad W_{2c0}\quad W_{3c0}\,]^{\mathrm{T}} \tag{27g}$$

$$\mathbf{Q}_{c0}=[\,Q_{1c0}\quad Q_{2c0}\quad Q_{3c0}\,]^{\mathrm{T}} \tag{27h}$$

The coefficients in Eqs. (27b), (27c), (27d), (27e) and (27f) are written as

$$l_{iit}=EA_{i\psi t}\omega_{it}-EB_{i\psi t}\rho_{it}+EI_{i\psi t};\ i=1,2,3 \tag{28a}$$

$$l_{jit}=EA_{j\psi t}\omega_{it}-EB_{j\psi t}\rho_{it};\ i=1,2,3,\ j=1,2,3,\ i\neq j \tag{28b}$$

$$m_{jt}=GI_{jd\psi t};\ j=1,2,3 \tag{28c}$$

$$n_{pjt}=EB_{j\psi t}\rho_{pt}-EA_{j\psi t}\omega_{pt};\ j=1,2,3 \tag{28d}$$

$$n_{Nj}=EB_{j\psi t}\rho_{Nt}-EA_{j\psi t}\omega_{Nt};\ j=1,2,3 \tag{28e}$$

$$n_{Mj}=EB_{j\psi t}\rho_{Mt}-EA_{j\psi t}\omega_{Mt};\ j=1,2,3 \tag{28f}$$

Compared with Eq. (19), the added terms in Eq. (26) related to the stress resultants at time $t_0$ is due to the constitutive relationship of concrete creep. On the basis of Eq. (14), the expressions of the stress resultants at time $t_0$ can be determined as

$$N_{c0}=\sum_{\alpha=1}^{3}(a_{N(2\alpha-1)}\,\mathrm{sh}\,\lambda_{\alpha0}z+a_{N(2\alpha)}\,\mathrm{ch}\,\lambda_{\alpha0}z)+a_{N7}z^2+a_{N8}z+a_{N9} \tag{29a}$$

$$M_{c0}=\sum_{\alpha=1}^{3}(a_{M(2\alpha-1)}\,\mathrm{sh}\,\lambda_{\alpha0}z+a_{M(2\alpha)}\,\mathrm{ch}\,\lambda_{\alpha0}z)+a_{M7}z^2+a_{M8}z+a_{M9} \tag{29b}$$

$$W_{ic0}=\sum_{\alpha=1}^{3}(a_{Wi(2\alpha-1)}\,\mathrm{sh}\,\lambda_{\alpha0}z+a_{Wi(2\alpha)}\,\mathrm{ch}\,\lambda_{\alpha0}z)+a_{Wi7}z^2+a_{Wi8}z+a_{Wi9};\ i=1,2,3 \tag{29c}$$

$$Q_{ic0}=\sum_{\alpha=1}^{3}(a_{Qi(2\alpha-1)}\,\mathrm{ch}\,\lambda_{\alpha0}z+a_{Qi(2\alpha)}\,\mathrm{sh}\,\lambda_{\alpha0}z)+a_{Qi7}z+a_{Qi8};\ i=1,2,3 \tag{29d}$$

where the coefficients $a_{Nl}$, $a_{Ml}$, $a_{Wil}$ and $a_{Qim}$ ($l$=1, ..., 9; $m$=1, ..., 8) can be achieved in the shear lag analysis at time $t_0$.

In accordance with Eq. (26), the closed-form solutions of $f_{it}$ can be expressed as

$$f_{it}=\sum_{\alpha=1}^{3}\xi_{i\alpha t}(C_{(2\alpha-1)t}\,\mathrm{ch}\,\lambda_{\alpha t}z+C_{(2\alpha)t}\,\mathrm{sh}\,\lambda_{\alpha t}z)-\frac{n_{pit}}{m_{it}}(p_y z+C_t)+f_{itp};\ i=1,2,3 \tag{30}$$

and

$$\boldsymbol{\xi}_t=\begin{bmatrix}\xi_{11t} & \xi_{12t} & \xi_{13t}\\ \xi_{21t} & \xi_{22t} & \xi_{23t}\\ \xi_{31t} & \xi_{32t} & \xi_{33t}\end{bmatrix} \tag{31}$$

where $C_{kt}$ ($k$=1, ..., 6) are the integral constants, which can be calculated based on the boundary conditions at time $t$; $\lambda_{\alpha t}^2$ ($\alpha$=1, 2, 3) are the eigenvalues of $\mathbf{L}_t^{-1}\mathbf{M}_t$; $\boldsymbol{\xi}_t$ is the matrix of the right eigenvetors of $\mathbf{L}_t^{-1}\mathbf{M}_t$.

By taking advantage of Eq. (29), the particular solutions, which only depend on the stress resultants at time $t_0$, can be derived as

$$\mathbf{f}_{tp}=\sum_{\alpha=1}^{3}(\boldsymbol{\eta}_{(2\alpha-1)}\,\mathrm{ch}\,\lambda_{\alpha0}z+\boldsymbol{\eta}_{(2\alpha)}\,\mathrm{sh}\,\lambda_{\alpha0}z)+\boldsymbol{\eta}_7 z+\boldsymbol{\eta}_8 \tag{32}$$

and

$$\mathbf{f}_{tp} = [\, f_{1tp} \quad f_{2tp} \quad f_{3tp}\,]^{\mathrm{T}} \tag{33a}$$

$$\boldsymbol{\eta}_{(2\alpha-1)} = \mathbf{H}(\lambda_{\alpha 0} a_{N(2\alpha-1)} \mathbf{N}_N + \lambda_{\alpha 0} a_{M(2\alpha-1)} \mathbf{N}_M - \lambda_{\alpha 0} \phi \mathbf{a}_{W(2\alpha-1)} + \phi \mathbf{a}_{Q(2\alpha-1)}); \alpha = 1, 2, 3 \tag{33b}$$

$$\boldsymbol{\eta}_{(2\alpha)} = \mathbf{H}(\lambda_{\alpha 0} a_{N(2\alpha)} \mathbf{N}_N + \lambda_{\alpha 0} a_{M(2\alpha)} \mathbf{N}_M - \lambda_{\alpha 0} \phi \mathbf{a}_{W(2\alpha)} + \phi \mathbf{a}_{Q(2\alpha)}); \alpha = 1, 2, 3 \tag{33c}$$

$$\boldsymbol{\eta}_7 = -\mathbf{M}_t^{-1}(2a_{N7}\mathbf{N}_N + 2a_{M7}\mathbf{N}_M - 2\phi \mathbf{a}_{W7} + \phi \mathbf{a}_{Q7}) \tag{33d}$$

$$\boldsymbol{\eta}_8 = -\mathbf{M}_t^{-1}(a_{N8}\mathbf{N}_N + a_{M8}\mathbf{N}_M - \phi \mathbf{a}_{W8} + \phi \mathbf{a}_{Q8}) \tag{33e}$$

where

$$\mathbf{H} = (\lambda_{\alpha 0}^2 \mathbf{L}_t - \mathbf{M}_t)^{-1}; \alpha = 1, 2, 3 \tag{34}$$

In particular, it should be noted that the solutions of the generalized displacements obtained by the proposed method can be reduced to those obtained from the elementary beam theory if the shear lag effect is ignored.

## 3. Numerical applications

Two case studies of a simply-supported RC box girder and a continuous RC box girder are presented below. The short- and long-term results computed by the proposed method for the simply-supported girder are compared with those calculated by the finite element method and the elementary beam theory. Moreover, creep analyses with and without shrinkage are conducted for an evaluation of time effects on the long-time behavior of the continuous girder.

### *3.1 Verification of the proposed method*

With the development of bridge engineering, box girders with long cantilever slabs and large-spacing webs have been widely used. Shear lag effect in these box girders is more evident than that in general box girders. Fig. 4 shows a scaled (1:6) simply-supported RC box girder which was provided by Cao (2000). It is assumed that the load $p_y$=21.2 kN/m is applied at 28 days from casting of the concrete, namely, $t_0$=28 days. The final time of the analysis is $t$=3628 days. And the age of the concrete at the beginning of shrinkage, $t_s$, is taken as 3 days. Young's modulus of the concrete at time $t_0$ is $E_{c0}$=32.6 GPa, and Poisson's ratio is $\mu$=0.167. The mean compressive strength of the concrete at the age of 28 days, $f_{cm}$, is 37.4 MPa. The relative humidity is $RH$=70%. Young's modulus of the reinforcements is $E_r$=210 GPa. The creep and shrinkage functions can be determined in terms of CEB-FIP model code 1990 (1993). For the convenient calculation of the aging coefficient $\chi$, the different simplified expressions for $\chi$ were provided by the literature (Lacidogna and Tarantino 1996, Jirasek and Bazant 2002). Moreover, a step-by-step method, which was presented by Bazant (1972) and programmed by Ghali *et al.* (2012), is adopted to obtain a more accurate value of $\chi$ in this paper. In view of the length limitation, the computer code for $\chi$ given by Ghali *et al.* (2012) is not listed here.

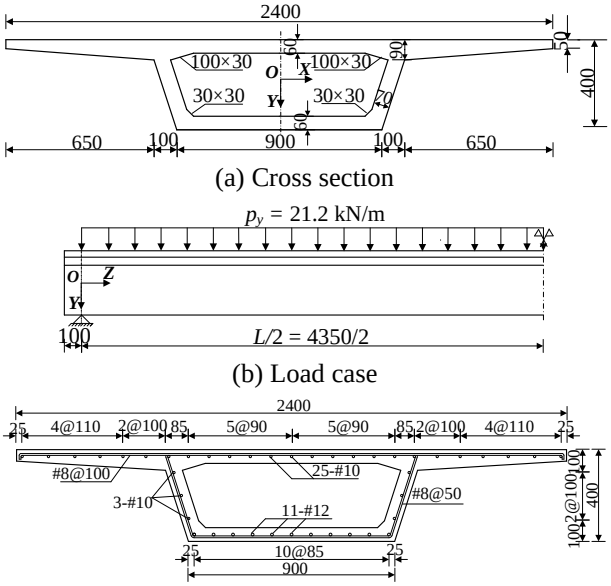


Fig. 4 Simply-supported RC box girder (unit: mm)

In this paper, the software MIDAS is used for the finite element analysis of the box girder. As shown in Fig. 5, the finite element model, which can automatically capture the shear lag effect, is constructed using eight-node solid elements. The longitudinal reinforcements and stirrups can be modeled as line elements, attached to the concrete at the nodes. Besides, the time-varying behavior of the box girder can be obtained by the step-by-step method.

Fig. 6(a) depicts the deflections of the box girder calculated by various methods at times $t_0$ and $t$. EBT, SSL, SLCS and FEA represent the analyses based on the elementary beam theory, the short-term analysis of shear lag, the shear-lag analysis considering creep and shrinkage, and the finite element analyses, respectively. Compared with the proposed method considering shear lag, the analyses based on the elementary beam theory underestimate the mid-span deflections at both time $t_0$ and time $t$ by about 11%. The deflections obtained by the proposed method are relatively close to those calculated by the finite element method. The small differences between these two approaches are mainly caused by the shear deformations of the webs which are ignored in the proposed method. As shown in Fig. 6(b), the mid-span deflections resulting from creep and shrinkage at time $t$ computed by each method are about twice larger than those at time $t_0$.

Fig. 7 shows the time-varying transverse distributions of the axial stresses in the top and bottom slabs at mid-span. It is observed that both the short- and long-term stresses in the flanges obtained from the proposed method are in very good agreement with those from the finite element analyses. Because of the neglect of the shear lag effect, the longitudinal stresses computed by the elementary beam

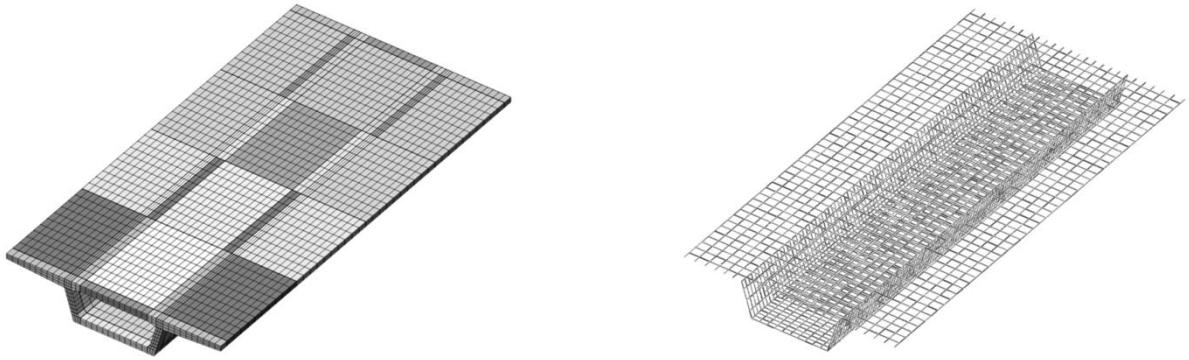

(a) Concrete (b) Reinforcement

Fig. 5 Finite element model for simply-supported box girder

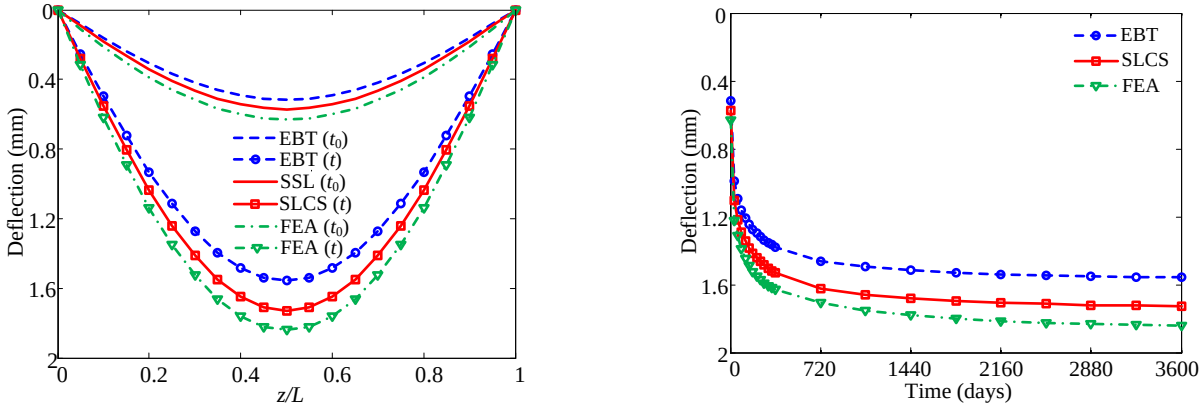


(a) Deflection curves (b) Mid-span deflections

Fig. 6 Time evolution of deflections of simply-supported box girder

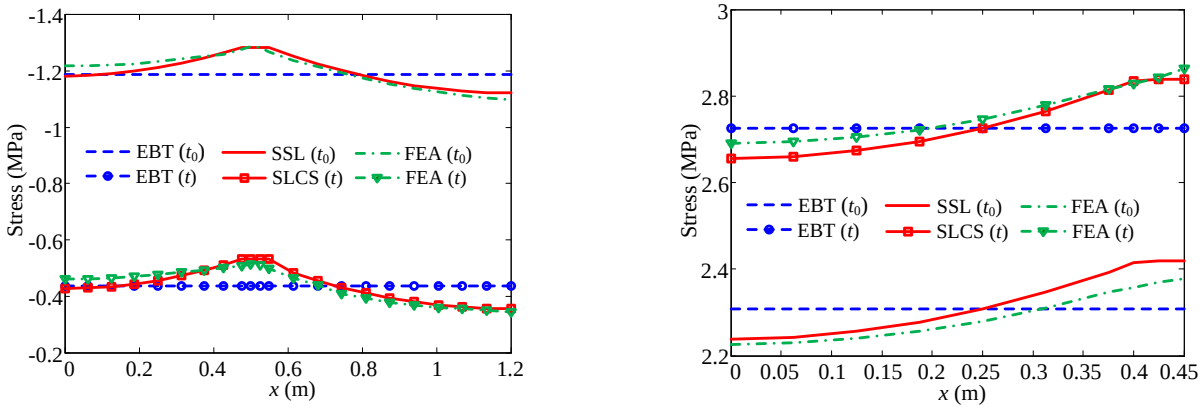


(a) Top slab (b) Bottom slab

Fig. 7 Transverse distributions of axial stresses at mid-span of simply-support box girder

theory are uniformly distributed, leading to considerable errors in the stress calculations (Kristek and Kadlec 2014).

As shown in Fig. 7(a), a reduction with time of the compressive stresses is obvious in the top slab, owing to the creep and shrinkage. On the other hand, Fig. 7(b) shows that the tensile stresses in the bottom slab gradually increases with time. The stresses in the top and bottom slabs gradually get close to 0 and tensile strength of the concrete, respectively. Therefore, the time evolution of the stresses in the top and bottom plates is detrimental to the girder. Moreover, in the case of constant external loads, creep and shrinkage generally cause the variation of stress values, and cannot substantially modify the shape of the transverse distributions of axial stresses (Xiang and He 2015).

### *3.2 Creep analyses with and without shrinkage*

A two-span continuous RC box girder, as shown in Fig. 8, is chosen to conduct the further analyses. Young's modulus of the concrete at time $t_0$ is $E_{c0}$=38.1 GPa. The mean compressive strength of the concrete at the age of 28 days is $f_{cm}$=48 MPa. The remaining parameters are the same as those of the simply-supported RC box girder in Section 3.1. The aging coefficient, creep and shrinkage functions are also calculated by the same method in Section 3.1.

In order to further elaborate the effects of creep and shrinkage on the structural responses, two different shear-lag analyses, including creep analysis with shrinkage (SLCS) and creep analysis without shrinkage (SLC), are carried out for the continuous box girder.

The differences of the deflection curves obtained from creep analyses with and without shrinkage are shown in Fig. 9(a). At time *t*, the deflection increment at mid-span due to creep accounts for about 81% of that due to creep and shrinkage. It illustrates that concrete creep has a greater impact on the long-term deflections than concrete shrinkage. The time-varying deflections of the box girder at mid-span are also plotted in Fig. 9(b). Although the impact of the concrete shrinkage on the long-term deflections becomes larger with time, the concrete creep is still dominant.

Fig. 10 plots the transverse distributions of the axial stresses in the top and bottom slabs at the interior support. Both creep and shrinkage can result in the reduction of the compressive stresses in the bottom slab. Besides, the reduction and increase of the tensile stresses in the top plate are caused by creep and shrinkage, respectively. It can be seen that concrete creep may mainly induce the stress migration from the concrete to the reinforcing bars, while concrete shrinkage may trigger the cracking in the top slab in tension. Therefore, not only creep but also shrinkage should be paid attention to in the stress analysis of concrete box girders.

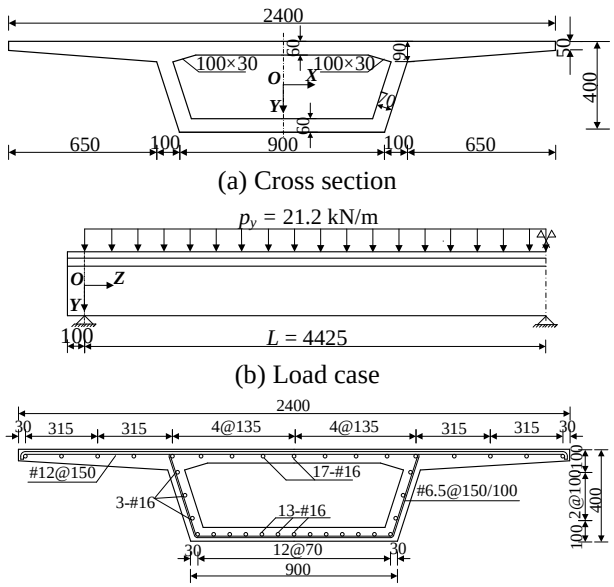


(a) Cross section

(b) Load case

(c) Reinforcement arrangement

Fig. 8 Two-span continuous RC box girder (unit: mm)

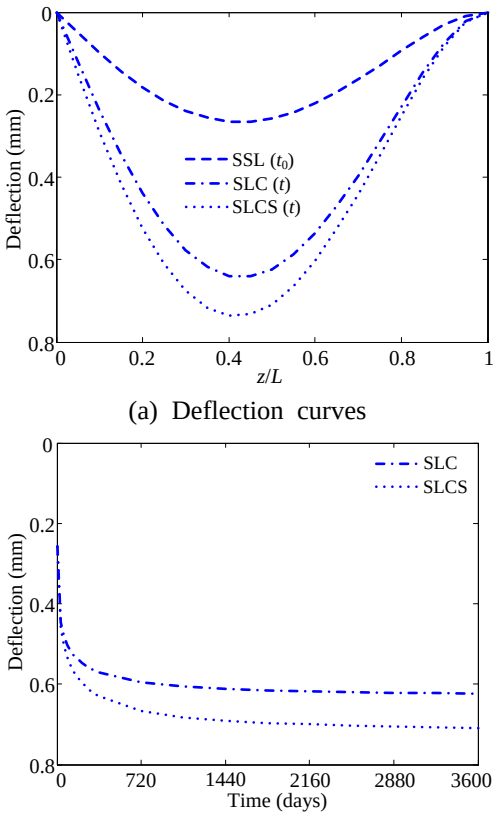


(a) Deflection curves

(b) Mid-span deflections

Fig. 9 Time evolution of deflections of continuous box girder

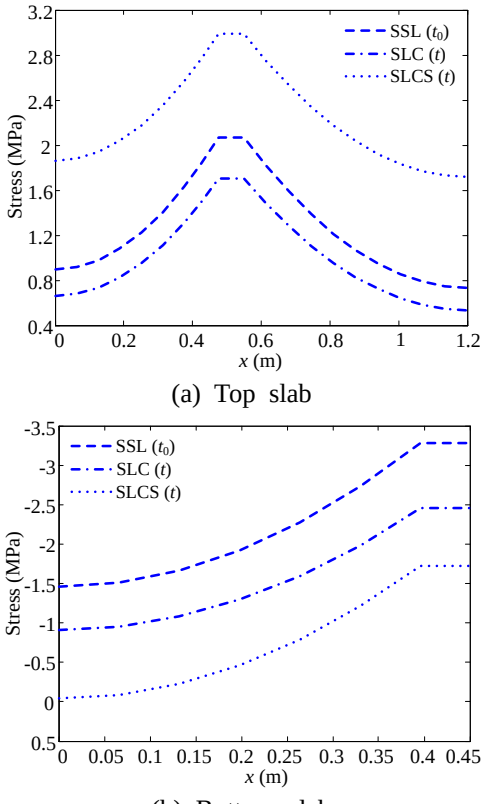


(a) Top slab

(b) Bottom slab

Fig. 10 Transverse distributions of axial stresses at interior support of continuous box girder

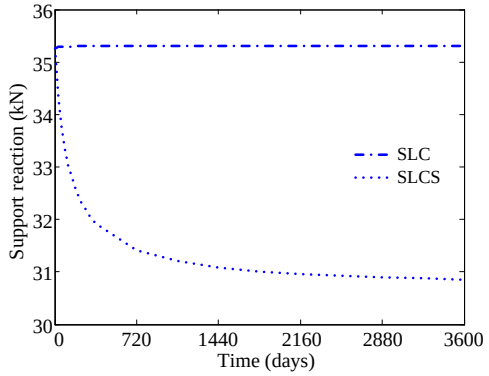


(a) End support

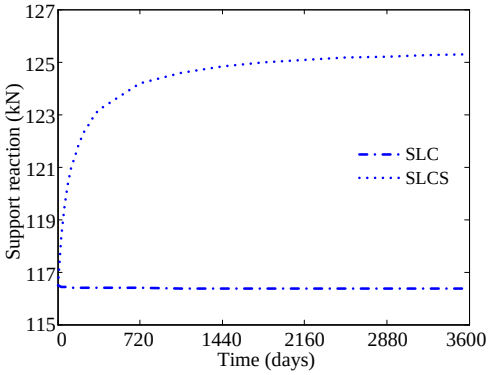


(b) Interior support

Fig. 11 Time evolution of support reactions in continuous box girder

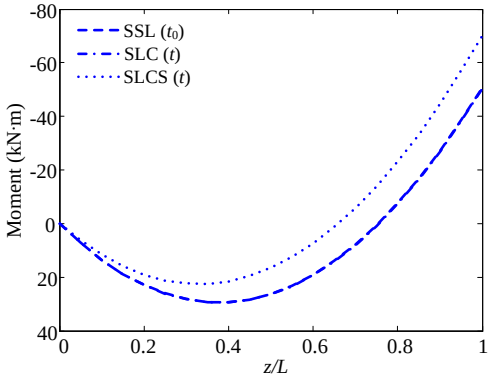


(a) Distributions of moments

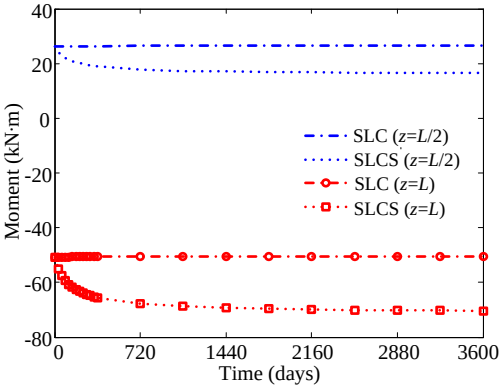


(b) Moments at mid-span and at interior support

Fig. 12 Time evolution of bending moments in continuous box girder

The variations of support reactions and bending moments due to time effects are reported in Figs. 11-12, respectively. Concrete creep has virtually no effect on the support reactions and the bending moments. It is also observed that the reaction at the interior support increases while the reaction at the end support reduces because of concrete shrinkage. Hence, the hogging moment at the interior support increases while the sagging moment at mid-span decreases. The similar variations with time were also observed by Lou *et al*. (2014). At 3628 days, the concrete shrinkage decreases the reaction at the end support and the moment at mid-span by approximately 12.5% and 37.0%, respectively. Therefore, time effects on the redistribution of internal forces and support reactions should be attached importance to in statically indeterminate concrete structures.

## 4. Conclusions

An analytical model considering axial equilibrium is developed for analyzing the short- and long-term shear lag effect in reinforced concrete box girders. In order to take into account the axial equilibrium, the longitudinal displacement of the web is added to the displacement field. Three independent shear lag functions are applied to denote the different shear lag intensities of the top, bottom and cantilever slabs, respectively. The age-adjusted effective modulus method is adopted for modeling the time-dependent behavior of the concrete. The governing system of differential equations and corresponding boundary conditions can be determined based on the virtual work theorem and the partial integration. The closed-form solutions of the short- and long-term behavior are derived for concrete box girders subjected to uniformly distributed loads. Meanwhile, the proposed method is employed to investigate the short- and long-term responses of a simply-supported RC box girder. The results obtained by the proposed method are compared with those from the traditional elementary beam theory and the finite element analyses. In addition, creep analyses with and without shrinkage are also performed for quantifying the effects of creep and shrinkage on the long-term behavior of a continuous RC box girder.

The following conclusions could be drawn:

• Both the short- and long-term responses calculated by the presented model are in good agreement with those obtained from the finite element analyses. Compared with the proposed method, the conventional analyses based on the elementary beam theory lead to significant errors in the prediction of the structural responses.

• Creep has a significant impact on the long-term deflections, while shrinkage has a large effect on the concrete stresses. Moreover, it should be noted that shrinkage can remarkably affect the redistribution of the internal forces and support reactions in the continuous girder.

• It is quite necessary to comprehensively consider shear lag effect, creep and shrinkage in the long-term analysis of RC box girders. Especially at the design stage, the

proposed method is an effective tool for engineers to analyze the short- and long-term behavior of shear lag effect in RC box girders. Further extensive experimental studies should be conducted to calibrate the proposed method.

## Acknowledgments

The research described in this paper was financially supported by the National Natural Science Foundation of China under Grant No. 51178416.

## References

Bazant, Z.P. (1972), "Prediction of concrete creep effects using age-adjusted effective modulus method", *ACI J.*, **69**(4), 212-217.

Bazant, Z.P., Yu, Q. and Li, G.H. (2012a), "Excessive long-time deflections of prestressed box girders. I: Record-span bridge in Palau and other paradigms", *J. Struct. Eng.*, ASCE, **138**(6), 676-686.

Bazant, Z.P., Yu, Q. and Li, G.H. (2012b), "Excessive long-time deflections of prestressed box girders. II: Numerical analysis and lessons learned", *J. Struct. Eng.*, ASCE, **138**(6), 687-696.

Cao, G.H. (2000), "Analysis and experimental study on shear lag effect of RC box girder", M.Sc. Dissertation, Hunan University, Changsha, China. (in Chinese)

CEB-FIP model code 1990 (1993), Model Code for Concrete Structures, Euro-International Committee for Concrete-International Federation for Prestressing; Lausanne, Switzerland.

Dezi, L. and Mentrasti, L. (1985), "Nonuniform bending-stress distribution (shear lag)", *J. Struct. Eng.*, ASCE, **111**(12), 2675-2690.

Dezi, L., Gara, F. and Leoni, G. (2003), "Shear-lag effect in twin-girder composite decks", *Steel Compos. Struct.*, **3**(2), 111-122.

Dezi, L., Gara, F., Leoni, G. and Tarantino, A.M. (2001), "Time-dependent analysis of shear-lag effect in composite beams", *J. Eng. Mech.*, ASCE, **127**(1), 71-79.

Elbadry, M., Ghali, A. and Gayed, R.B. (2014), "Deflection control of prestressed box girder bridges", *J. Bridge Eng.*, ASCE, **19**(5), 04013027.

Gara, F., Leoni, G. and Dezi, L. (2009), "A beam element including shear lag effect for the time-dependent analysis of steel-concrete composite decks", *Eng. Struct.*, **31**(8), 1888-1902.

Gara, F., Ranzi, G. and Leoni, G. (2010), "Short- and long-term analytical solutions for composite beams with partial interaction and shear-lag effects", *Int. J. Steel Struct.*, **10**(4), 359-372.

Ghali, A., Favre, R. and Elbadry, M. (2012), *Concrete Structures: Stresses and Deformations, Analysis and Design for Serviceability*, (4th Edition), Spon Press, London, UK.

Gilbert, R.I. and Ranzi, G. (2011), *Time-dependent Behavior of Concrete Structures*, Spon Press, London, UK.

Granata, M.F., Margiotta, P. and Arici, M. (2013), "Simplified procedure for evaluating the effects of creep and shrinkage on prestressed concrete girder bridges and the application of European and North American prediction models", *J. Bridge Eng.*, ASCE, **18**(12), 1281-1297.

Guo, T. and Chen, Z.H. (2016), "Deflection control of long-span PSC box-girder bridge based on field monitoring and probabilistic FEA", *J. Perform. Constr. Facil.*, ASCE, **30**(6), 04016053.

Jirasek, M. and Bazant, Z.P. (2002), *Inelastic Analysis of Structures*, Wiley, Chichester, UK.

Kristek, V. and Bazant, Z.P. (1987), "Shear lag effect and uncertainty in concrete box girder creep", *J. Struct. Eng.*, ASCE, **113**(3), 557-574.

Kristek, V. and Kadlec, L. (2014), "The cross-section warping effect with the associated creep-induced deformations", *Adv. Eng. Softw.*, **72**, 213-217.

Lacidogna, G. and Tarantino, M. (1996), "Approximate expressions for the ageing coefficient and the relaxation function in the viscoelastic analysis of concrete structures", *Mater. Struct.*, **29**(3), 131-140.

Lin, Z.B. and Zhao, J. (2011a), "Least-work solutions of flange normal stresses in thin-walled flexural members with high-order polynomial", *Eng. Struct.*, **33**(10), 2754-2761.

Lin, Z.B. and Zhao, J. (2011b), "Revisit of AASHTO effective flange-width provisions for box girders", *J. Bridge Eng.*, ASCE, **16**(6), 881-889.

Lou, T.J., Lopes, S.M.R. and Lopes, A.V. (2014), "A finite element model to simulate long-term behavior of prestressed concrete girders", *Finite Elem. Anal. Des.*, **81**, 48-56.

Lou, T.J., Lopes, S.M.R. and Lopes, A.V. (2015a), "FE analysis of short- and long-term behavior of simply supported slender prestressed concrete columns under eccentric end axial loads causing uniaxial bending", *Eng. Struct.*, **85**, 52-62.

Lou, T.J., Lopes, S.M.R. and Lopes, A.V. (2015b), "Interaction between time-dependent and second-order effects of externally posttensioned members", *J. Bridge Eng.*, ASCE, **20**(11), 06015003.

Lou, T.J., Lopes, S.M.R. and Lopes, A.V. (2016), "Time-dependent behavior of concrete beams prestressed with bonded AFRP tendons", *Compos. Part B: Eng.*, **97**, 1-8.

Luo, Q.Z., Wu, Y.M., Li, Q.S., Tang, J. and Liu, G.D. (2004), "A finite segment model for shear lag analysis", *Eng. Struct.*, **26**(14), 2113-2124.

Malm, R. and Sundquist, H. (2010), "Time-dependent analyses of segmentally constructed balanced cantilever bridges", *Eng. Struct.*, **32**(4), 1038-1045.

Norachan, P., Kim, K.D. and Onate, E. (2014), "Analysis of segmentally constructed prestressed concrete bridges using hexahedral elements with realistic tendon profiles", *J. Struct. Eng.*, ASCE, **140**(6), 04014028.

Pan, Z.F., Fu, C.C. and Jiang, Y. (2011), "Uncertainty analysis of creep and shrinkage effects in long-span continuous rigid frame of Sutong Bridge", *J. Bridge Eng.*, ASCE, **16**(2), 248-258.

Reissner, E. (1946), "Analysis of shear lag in box beams by the principle of the minimum potential energy", *Q. Appl. Math.*, **4**(3), 268-278.

Robertson, I.N. (2005), "Prediction of vertical deflections for a long-span prestressed concrete bridge structure", *Eng. Struct.*, **27**(12), 1820-1827.

Sousa, C., Sousa, H., Neves, A.S. and Figueiras, J. (2012), "Numerical evaluation of the long-term behavior of precast continuous bridge decks", *J. Bridge Eng.*, ASCE, **17**(1), 89-96.

Sousa, H., Bento, J. and Figueiras, J. (2014), "Assessment and management of concrete bridges supported by monitoring data-based finite-element modeling", *J. Bridge Eng.*, ASCE, **19**(6), 05014002.

Takacs, P.F. (2002), "Deformations in concrete cantilever bridges: Observations and theoretical modelling", Ph.D. Dissertation, The Norwegian University of Science and Technology, Trondheim, Norway.

Wen, Q.J. (2011), "Long-term effect analysis of prestressed concrete box-girder bridge widening", *Constr. Build. Mater.*, **25**(4), 1580-1586.

Wu, Y.P., Liu, S.Z., Zhu, Y.L. and Lai, Y.M. (2003), "Matrix analysis of shear lag and shear deformation in thin-walled box beams", *J. Eng. Mech.*, ASCE, **129**(8), 944-950.

Xiang, Y.Q. and He, X.Y. (2015), "Time-dependent behavior of PC box girder bridges considering non-uniform shrinkage and

creep", *J. Harbin Inst. Tech.*, **47**(12), 117-122. (in Chinese)
Xiang, Y.Q., Tang, G.B. and Liu, C.X. (2011), "Cracking mechanism and simplified design method for bottom flange in prestressed concrete box girder bridge", *J. Bridge Eng.*, ASCE, **16**(2), 267-274.
Yang, I.H. (2007a), "Uncertainty and sensitivity analysis of time-dependent effects in concrete structures", *Eng. Struct.*, **29**(7), 1366-1374.
Yang, I.H. (2007b), "Prediction of time-dependent effects in concrete structures using early measurement data", *Eng. Struct.*, **29**(10), 2701-2710.
Zhang, Y.H. (2012), "Improved finite-segment method for analyzing shear lag effect in thin-walled box girders", *J. Struct. Eng.*, ASCE, **138**(10), 1279-1284.
Zhang, Y.H. and Lin, L.X. (2014a), "Shear lag analysis of thin-walled box girders adopting additional deflection as generalized displacement", *J. Eng. Mech.*, ASCE, **140**(4), 04014005.
Zhang, Y.H. and Lin, L.X. (2014b), "Shear lag analysis of thin-walled box girders based on a new generalized displacement", *Eng. Struct.*, **61**, 73-83.
Zhou, S.J. (2010), "Finite element considering shear-lag effect in box girder", *J. Eng. Mech.*, ASCE, **136**(9), 1115-1122.

*CC*